An Experimental and Theoretical Study of the Reactions OIO + NO and OIO + OH

J. M. C. Plane,*,[†] D. M. Joseph,[†] B. J. Allan,[†] S. H. Ashworth,[‡] and J. S. Francisco[§]

School of Environmental Sciences, University of East Anglia, Norwich NR4 7TJ, U.K., School of Chemical Sciences and Pharmacy, University of East Anglia, Norwich NR4 7TJ, U.K., and Department of Chemistry, Purdue University, West Lafayette, Indiana 47907-2084

Received: September 21, 2005; In Final Form: November 8, 2005

The kinetics of the reaction OIO + NO were studied by pulsed laser photolysis/time-resolved cavity ring-down spectroscopy, yielding $k(235-320\ \mathrm{K}) = 7.6^{+4.0}{}_{-3.1} \times 10^{-13} \exp[(607\pm128)/T]$ cm^3 molecule^{-1} s^{-1}. Quantum calculations on the OIO + NO potential-energy surface show that the reactants form a weakly bound OIONO intermediate, which then dissociates to the products IO + NO_2. Rice−Ramsberger−Kassel−Markus (RRKM) calculations on this surface are in good accord with the experimental result. The most stable potential product, $IONO_2$, cannot form because of the significant rearrangement of OIONO that would be required. The reaction OIO + OH was then investigated by quantum calculations of the relevant stationary points on its potential-energy surface. The very stable $HOIO_2$ molecule can form by direct recombination, but the bimolecular reaction channels to HO_2 + IO and HOI + O_2 are closed because of significant energy barriers. RRKM calculations of the $HOIO_2$ recombination rate coefficient yield $k_{\mathrm{rec},0} = 1.5 \times 10^{-27} (T/300\ \mathrm{K})^{-3.93}$ cm^6 molecule^{-2} s^{-1}, $k_{\mathrm{rec},\infty} = 5.5 \times 10^{-10} \exp(46/T)$ cm^3 molecule^{-1} s^{-1}, and $F_c = 0.30$. The rate coefficients of both reactions are fast enough around 290 K and 1 atm pressure for these reactions to play a potentially important role in the gas phase and aerosol chemistry in the marine boundary layer of the atmosphere.

Introduction

Observations of the iodine oxide radicals IO[1−3] and OIO[3,4] in the marine boundary layer have established the importance of iodine chemistry in the lower troposphere. Iodine can have several major impacts, including the destruction of ozone,[5−7] the activation of chlorine and bromine from sea salt,[7,8] the removal of nitrogen oxides in semi-polluted air masses,[6] and the formation of ultrafine iodine oxide aerosol.[9−11]

The major sources of iodine in the marine boundary layer appears to be iodocarbons of biogenic origin such as CH_3I and CH_2I_2, which evade from the ocean,[12] and I_2, which is released from macroalgae exposed at low tide.[3] Following photolysis of these species to yield atomic I, the iodine oxide radical (IO) is produced by reaction with O_3. The OIO radical can form either through the self-reaction of IO

$$\mathrm{IO + IO \rightarrow OIO + I} \tag{1}$$

which has a yield of around 30−50%,[13,14] or through the reaction[15]

$$\mathrm{BrO + IO \rightarrow OIO + Br} \tag{2}$$

Observations of OIO by the technique of differential optical absorption spectroscopy[3,4] showed that during daytime the OIO mixing ratio was consistently below the instrumental detection limit of ~3 parts per trillion (ppt, where 1 ppt = 2.5×10^7 molecule cm^{-3} at 290 K and 1 atm pressure), using a new absolute cross section for OIO.[14] Since the daytime IO mixing ratio tends to be around 5 ppt,[1−3] a steady-state calculation using reaction 1 indicates that the lifetime of OIO during the day must be less than about 140 s.

There appear to be two possible explanations for this absence of OIO during daytime. First, it could photolyze following absorption in the strong bands between about 470 and 610 nm. Although there is some experimental evidence for photolysis,[16] we have recently shown that absorption leads to internal conversion into the highly vibrationally excited ground state rather than dissociation, so the quantum yield for photolysis is probably much less than 10% at 562 nm.[14] Nevertheless, a small probability of photolysis, integrated over the absorption bands, could still account for the removal of OIO during daytime.[17]

A second possibility is that OIO is removed during daytime by reaction with radicals that have marked diurnal cycles with daytime maxima, such as NO, OH, and IO. We have shown in a recent modeling study[17] that the recombination of IO with OIO to make I_2O_3 is probably a major pathway for the removal of OIO in environments where there are significant daytime IO concentrations, in particular, when there are large emissions of I_2 from macroalgae. In contrast, the reactions of OIO with NO and OH may be important over the open ocean, where the source flux of iodine precursors is lower. These reactions are the subject of this paper.

The reaction between OIO and NO could proceed via several channels

$$\mathrm{OIO + NO \rightarrow IO + NO_2} \qquad \Delta H_0 = -70\ \mathrm{kJ\ mol^{-1}} \tag{3a}$$

$$\mathrm{(+M) \rightarrow IONO_2} \qquad \Delta H_0 = -166\ \mathrm{kJ\ mol^{-1}} \tag{3b}$$

$$\mathrm{\rightarrow I + NO_3} \qquad \Delta H_0 = -50\ \mathrm{kJ\ mol^{-1}} \tag{3c}$$

$$\mathrm{\rightarrow INO + O_2(^1\Delta_g)} \qquad \Delta H_0 = -10\ \mathrm{kJ\ mol^{-1}} \tag{3d}$$

---

* To whom correspondence should be addressed. E-mail: j.plane@uea.ac.uk.

[†] School of Environmental Sciences, University of East Anglia.

[‡] School of Chemical Sciences and Pharmacy, University of East Anglia.

[§] Purdue University.

10.1021/jp055364y

where the reaction enthalpy changes are calculated from ab initio quantum theory described later in the paper. A fifth channel, OIO + NO → INO_2 + $O(^1D)$, is highly endothermic (ΔH_0 = 191 kJ mol^{-1}) and so is excluded from further consideration. Note that if the reaction proceeds via channel 3a, this leads to a null O_3-depleting cycle with reaction 1, because the NO_2 produced will photolyze to generate O and hence O_3, thereby canceling out the O_3 removed by the I atom produced in reaction 1. However, k_{3a} would have to be significantly faster than the rate coefficients for the analogous reactions of BrO and ClO[18,19] in order to account for the observed upper limit to the lifetime of OIO. For instance, in a very clean marine environment with [NO] less than 30 ppt, k_{3a} would need to be greater than ~1 × 10^{-11} cm^3 $molecule^{-1}$ s^{-1}. Although recombination to produce $IONO_2$ is the most exothermic channel of reaction 3, this pathway involves significant rearrangement.

The reaction between OIO and OH could also have several channels

$$\mathrm{OIO} + \mathrm{OH}\ (+\mathrm{M}) \rightarrow \mathrm{HOIO_2} \qquad \Delta H_0 = -204\ \mathrm{kJ\ mol^{-1}} \tag{4a}$$

$$\rightarrow \mathrm{IO} + \mathrm{HO_2} \qquad \Delta H_0 = -25\ \mathrm{kJ\ mol^{-1}} \tag{4b}$$

$$\rightarrow \mathrm{HOI} + \mathrm{O_2}(^1\Delta_g) \qquad \Delta H_0 = -128\ \mathrm{kJ\ mol^{-1}} \tag{4c}$$

where again the reaction enthalpy changes are calculated from ab initio quantum theory described below. Unlike reaction 3, the recombination pathway in reaction 4 involves simple attachment of the oxygen atom of OH to the iodine atom of OIO, to yield the most stable isomer of $HOIO_2$, whereas a recent theoretical study of the IO + HO_2 and HOI + O_2 potential surfaces has shown that these contain significant energy barriers.[20] Channel 4a is particularly interesting because this reaction oxidizes the iodine atom to the +5 oxidation state, forming the iodate ion. This ion is often the major form of iodine in marine aerosols (where iodine is heavily enriched compared to its abundance in seawater), but its source is unexplained.[21] Formation of $HOIO_2$ in the gas phase, followed by uptake on sea-salt aerosol, might provide an important route.

In this paper we will describe an experimental study of reaction 3 using a laser flash photolysis/time-resolved cavity ring-down (CRD) technique,[16] where k_3 was measured over a range of temperature and pressure. The experimental results are then modeled using ab initio calculations on the relevant potential energy surfaces, combined with Rice−Ramsberger−Kassel−Markus (RRKM) theory. An attempt to study reaction 4 was unsuccessful because the photochemical generation of OIO also produced significant concentrations of I_2 in the reactor, and the I_2 + OH reaction then dominated the removal of OH. Nevertheless, theory is used to predict the reaction pathways and to calculate a rate coefficient for reaction 4. Finally, the atmospheric relevance of both reactions is considered.

Experimental Section

The experimental system for producing OIO and monitoring its concentration by CRD spectroscopy has been described previously.[14,16] IO was formed by reacting CF_3I with O atoms produced by the photolysis of N_2O at 193 nm using an ArF excimer laser (fluence in the cell = (0.8−2.4) × 10^{16} photon cm^{-2}). The reagents were diluted with N_2 gas, which flowed into the ends of the 1.45 m long CRD cell and acted as curtains to protect the cavity mirrors (RMI, Boulder: reflectivity nominally greater than 0.999 at 565 nm). The probe beam was a Nd:YAG-pumped dye laser (Sirah Cobra) operating with rhodamine 6G dye, which provided a spectral resolution better than 0.2 cm^{-1} (~0.006 nm) in the 570−590-nm region. This beam was steered into the CRD cell, after using a wedged quartz beam splitter to pick off portions that were directed into an I_2 fluorescence cell and a Coherent Wavemaster for wavelength calibration. In the cell there was a 30-cm overlap between the excimer and dye laser beams. The laser radiation leaking out of the ring-down cavity was passed through a 485-nm cut-on filter and detected with a photomultiplier tube. The data were displayed on a LeCroy 9361C digital oscilloscope (300 MHz bandwidth, 2.5 GS/s) and captured on computer by fitting each ring-down signal to an exponential decay. The fluorescence from the I_2 cell and the wavelength measured by the Wavemaster were recorded simultaneously. The ring-down time of the empty cavity was also recorded so that the mirror reflectivities could be used to normalize the raw spectra. The ring-down time for the empty cavity was typically τ_0 = 750 ns, indicating that the mirror reflectivity was actually about 0.994%. This was routinely recorded at the start of a set of experiments, and the standard deviation of τ_0 for an average of 10 laser shots was consistently less than 1%.

The absorption spectra of OIO were contaminated with I_2 absorption to some degree, even though the gas residence time was kept short (0.7−1.4 s at 20 and 70 Torr, respectively), and the excimer laser was triggered at only 3 Hz to avoid the build-up of I_2 from the fast recombination of I atoms in this photochemical system.[14] OIO was also monitored at 567.808 nm, close to the peak in one of the OIO vibrational bands[14] but at a trough in the I_2 spectrum, to further minimize interference from I_2. The time-resolved variation of the OIO absorption was recorded using a scanned boxcar gate to trigger the dye laser. The baseline was recorded at long times after the excimer pulse (up to 3 ms) and then the absorption monitored as a function of time delay.

For the study of reaction 4, H_2 or H_2O was added to the CF_3I/N_2O mix flowing into the CRD cell. OH was then produced by the rapid reaction of $O(^1D)$, produced from the 193 nm photolysis of N_2O, with H_2 or H_2O, and also by the direct photolysis of H_2O at 193 nm. OH was then probed at 281.904 nm [$OH(A^2\Sigma - X^2\Pi)$, (1,0)] using a second dye laser orthogonal to the excimer and CRD laser beams. The time-resolved nonresonant laser induced fluorescence (LIF) at 307−312 nm [$OH(A^2\Sigma - X^2\Pi)$, (0,0)] was detected by a photomultiplier after passing through an interference filter at 307 ± 5 nm and captured by a gated integrator.

The central section of the CRD cell, containing the reaction volume where the excimer and CRD lasers overlapped, was enclosed in an insulated jacket through which ethanol was pumped through a temperature-controlled bath. This enabled the temperature of the gases in the reaction volume to be varied between 235 and 320 K, as measured by a chromel−alumel thermocouple that could be inserted into the center of the reactor.

Materials. CF_3I (99% pure, Fluorochem Ltd), N_2 (99.9999% pure, Air Products), H_2 (99.9999% pure, Air Products), and N_2O (99.99% pure, Air Products) were used without further purification. NO (99.9% pure, Air Products) was distilled from 77 K to remove traces of NO_2. MilliQ H_2O was freeze−pump−thawed for several cycles in a glass handling line and H_2O vapor then made up to a known ratio in about 760 Torr of bath gas in a glass bulb.

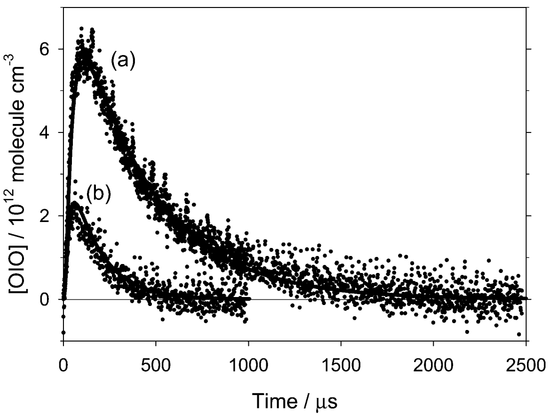

Figure 1. Typical OIO time profiles measured by CRD during the study of the reaction of OIO + NO. Experimental conditions: (a) [NO] = 2.78×10^{14} molecule cm^{-3} and (b) [NO] = 8.94×10^{14} molecule cm^{-3}; [CF_3I] = 1.34×10^{16} cm^{-3}; [N_2O] = 9.45×10^{16} cm^{-3}; [N_2] = 5.34×10^{17} cm^{-3}; $T = 300$ K. The solid lines are model calculations, which include a value for k_3 of 6.0×10^{-12} cm^3 molecule^{-1} s^{-1} obtained by fitting a single exponential to the OIO decay an appropriate interval after the peak (see text). The concentration of OIO is derived from the model assuming a branching ratio for OIO formation from the IO self-reaction of 0.32.

Experimental Results

Figure 1 illustrates time-resolved profiles of the OIO concentration at low and high concentrations of NO. The OIO absorbance measured by CRD was converted into absolute OIO concentration using our recently determined absorption cross section of $(1.5 \pm 0.18) \times 10^{-17}$ cm^2 at 567.93 nm.[14] Examples of OIO spectral scans between 558 and 578 nm using this CRD system are given in two previous papers.[14,16] Sufficiently high levels of IO were produced to ensure that OIO was formed essentially within 100 μs. In all experiments where NO was added, the removal of OIO was then dominated by reaction 3 and could be described at sufficiently long times after the peak by the pseudo-first-order decay coefficient

$$k' = k_{\mathrm{diff}} + k_3[\mathrm{NO}] \tag{I}$$

where k_{diff} includes diffusion of OIO out of the volume sampled by the dye laser and other removal processes (including reaction of OIO with the small amount of NO generated by the excimer laser through the reaction $O(^1D) + N_2O \rightarrow 2NO$). In these experiments, k_{diff} varied between 1800 and 5000 s^{-1}, depending on the excimer laser fluence and reagent concentrations. This ensured that $k_3[\mathrm{NO}] \gg k_{\mathrm{diff}}$. As expected, the decays were well fitted, after an appropriate time delay (20−50 μs after the peak of the OIO profile), by a single exponential form yielding k'. Figure 2 shows plots of k' vs [NO], along with linear regression fits to the data. The slopes of these plots yield k_3. Figure 2a shows measurements of k_3 at 300 K made at three different pressures (20, 40, and 72 Torr), which demonstrate that k_3 is independent of pressure within the experimental uncertainty. Figure 3b shows a selection of plots over the range of temperatures studied, illustrating that k_3 has a negative temperature dependence. Table 1 lists the measurements of k_3 as a function of temperature and pressure.

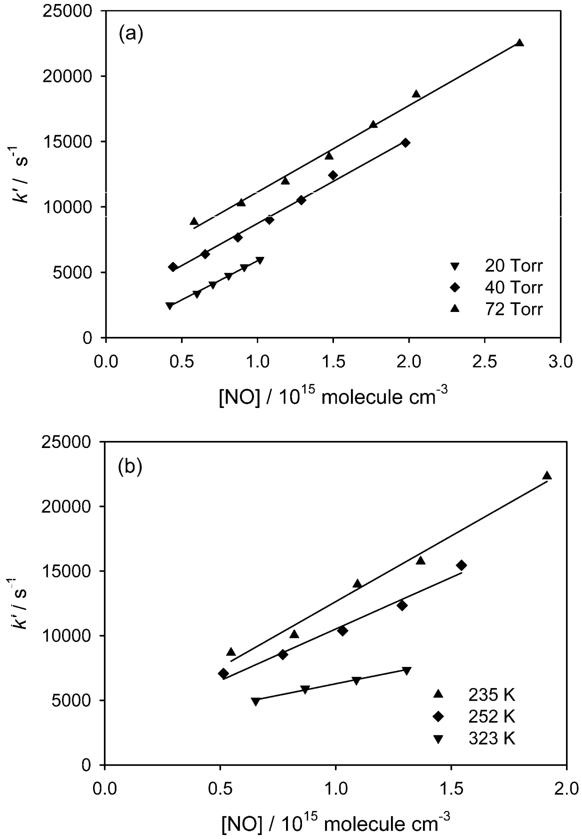

Figure 2. Plots of k' vs [NO]: (a) measurements at 300 K and pressures of 20, 40, and 72 Torr, where the data-sets at 40 and 72 Torr have been offset for clarity; (b) measurements at 40 Torr and 235, 252, and 323 K. The solid lines are linear least-squares fits through each set of data.

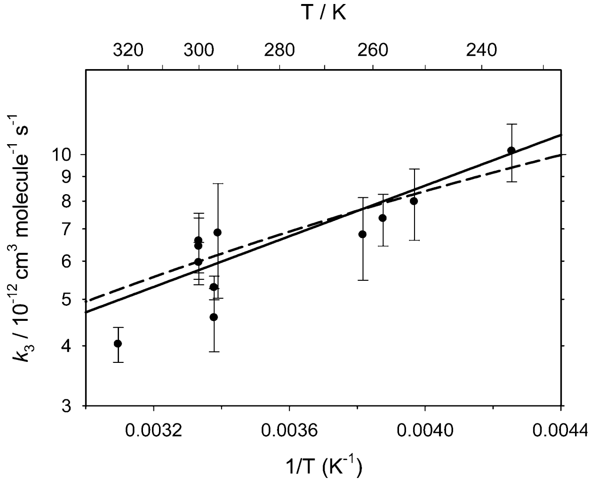

Figure 3. Arrhenius plot for reaction 3. The points are measurements of k_3 with 2σ error bars. The solid line is a linear regression through these points. The broken line is an RRKM fit to the data, using the potential-energy surface in Figure 4.

The solid lines fitted through the time profiles of [OIO] in Figure 1 are the predictions of a model that includes 38 reactions describing the chemistry in the reactor.[14] The model inputs are the temperature, pressure, [CF_3I], [N_2O], [NO], and the excimer laser fluence measured in the reactor. By use of k_3 derived above, the modeled OIO profile describes the experimental profiles very satisfactorily. The modeled absolute [OIO] is obtained by assuming a yield of 32% for OIO formation in reaction 1.[14] The use of the model confirms that fitting the decays after an appropriate delay to obtain k' is consistent with the removal of OIO at long reaction times being dominated by the large excess of NO in the reactor.

The model can also be used to examine the possible interference of CF_3 radicals in the measurement of k_3. CF_3 is produced by the reaction of O with CF_3I and, to a minor extent, by photolysis of CF_3I at 193 nm. The predicted [CF_3] reaches

TABLE 1: Measured Rate Coefficients (2σ Uncertainties) for the Reaction OIO + NO as a Function of Temperature

temperature (K)	rate coefficient k_3 (10^{-12} cm^3 molecule s^{-1})	pressure (Torr)
235	10.2 ± 1.4	40
252	8.0 ± 1.3	40
258	7.4 ± 0.9	40
262	6.8 ± 1.3	40
295	6.9 ± 1.8	40
296	5.3 ± 0.3	40
296	4.6 ± 0.7	40
300	6.0 ± 0.6	20
300	6.4 ± 0.9	40
300	6.6 ± 0.9	72
323	4.0 ± 0.3	40

a maximum of $\sim 8 \times 10^{13}$ cm^{-3} about 20 μs after the excimer pulse. We have shown previously[14] that the exothermic channels of a possible reaction between CF_3 and OIO would produce CF_3O + IO or CF_3OI + O. In both cases, IO would result and recycle back to OIO, thus not causing the rapid removal of OIO that is observed. Furthermore, the recombination of CF_3 and NO is quite rapid (7×10^{-12} cm^3 molecule^{-1} s^{-1} at 300 K and 40 torr N_2[22]). Thus, at the highest NO concentrations employed here, CF_3 would essentially be removed within 150 μs, which would have distorted the single exponential decays of OIO if CF_3 had a significant impact on the temporal behavior of OIO.

The other major byproduct in this system of OIO production is atomic I. We have shown recently[14] that in the absence of a reagent such as NO, the recombination of I with OIO appears to control the rate of OIO removal. i.e., $k_{\rm diff}$ in equation I. However, the model indicates that [I] should have increased by only ~25% at the maximum [NO] used in these experiments, so this would have had a minor effect on k' and the determination of k_3. A final point is that the predicted [NO_2] produced in the reactor would have been about 1.2×10^{13} cm^{-3} at the maximum added [NO] and thus much too small to cause any measurable absorbance in the CRD signal at 567.8 nm.

Figure 3 is an Arrhenius plot for reaction 3. An unweighted least-squares fit through the experimental data points yields (2σ errors)

$$k_3(235 - 320\ \mathrm{K}) = 7.6^{+4.0}_{-3.1} \times 10^{-13} \exp[(607 \pm 128)/T]\ \mathrm{cm^3\ molecule^{-1}\ s^{-1}} \qquad \mathrm{(II)}$$

The average rate coefficient at room temperature is k_3(298 K) = $(6.0 \pm 1.1) \times 10^{-12}$ cm^3 molecule^{-1} s^{-1}, where the quoted uncertainty of ±18% is estimated by combining in quadrature a 10% systematic error (comprising the sum of the uncertainties in the flow rates and total pressure) with a 15% standard deviation from the average of 6 room-temperature measurements.

When studying reaction 4, very rapid decays of OH (with first-order decay rates between 8 000 and 16 000 s^{-1}) were observed when CF_3I was added to the N_2O/H_2 mixture. Since the maximum concentration of OIO was only $\sim 6 \times 10^{12}$ cm^{-3} (Figure 1), the removal of OH was clearly not dominated by reaction 4. In fact, we have shown elsewhere that I_2 is produced by the recombination of I atoms in this system, perhaps facilitated by the iodine oxides acting as chaperones.[14] A spectral scan of the CRD laser in the 560−575-nm region, at a delay of more than 1 ms after the excimer when all the OIO has reacted away (Figure 1), enables the I_2 concentration to be measured. The concentration was typically $(4-8) \times 10^{13}$ cm^{-3}, which is consistent with the observed removal rate of OH, since k(OH + I_2) = 2.1×10^{-10} cm^3 molecule^{-1} s^{-1}.[23]

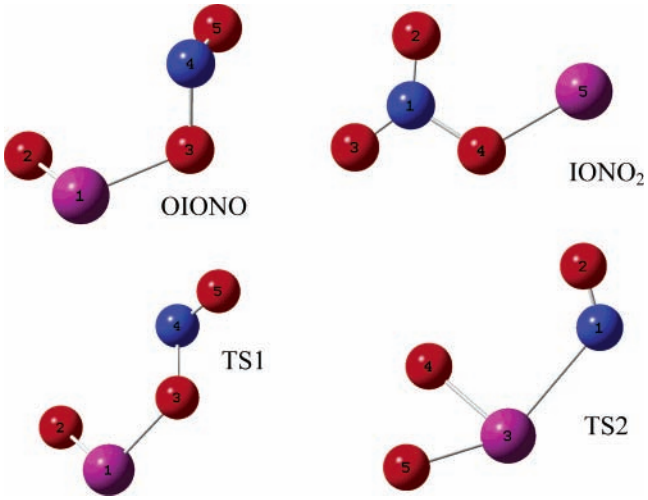

Figure 4. Geometries of stationary points on the OIO + NO potential-energy surface. The geometries are listed in Z matrix format in Table 2, and their relative energies are illustrated in Figure 5.

Quantum Calculations and Application of RRKM Theory. Ab initio quantum calculations were carried out to explore the reaction pathways of reactions 3 and 4. The hybrid density functional/Hartree−Fock B3LYP method was employed from within the Gaussian 03 suite of programs,[24] combined with a recently published basis set for I [25] and the standard 6-311+g(2d,p) triple-ζ basis set for O, N, and H. Following geometry optimizations of the relevant points on the potential-energy surfaces and the determination of their corresponding vibrational frequencies and (harmonic) zero-point energies, energies relative to the reactants were obtained. Spin−orbit corrections of −17 and −5 kJ mol^{-1} were applied to the B3LYP energies of I and IO, respectively. These were estimated by comparing the ab initio and the experimental bond energies (at 0 K) of I_2 and IO, which are taken as 148.8[26] and 236.0 kJ mol^{-1},[27] respectively.

Figure 4 illustrates the geometries of the stationary points on the resulting potential-energy surface of singlet spin multiplicity for the reaction OIO + NO; the geometries are described in Z matrix notation in Table 2. Figure 5 shows the potential-energy surface, and the ab initio rotational constants and vibrational frequencies for the relevant stationary points and asymptotes are listed in Table 3. For the reaction between OIO and OH, the stationary point geometries and potential-energy surface are shown in Figures 6 and 7, respectively. The Z matrix geometries are listed in Table 4 and rotational constants and vibrational frequencies in Table 5.

Rate coefficients for the relevant channels of reactions 3 and 4 were then estimated from RRKM theory, employing a Master Equation (ME) formalism with inverse Laplace transformation (ILT).[28] Reaction 3 is assumed to proceed via the formation of an excited adduct (OIONO*), which can either dissociate back to OIO + NO, be stabilized by collision with the third body (N_2) to form the OIONO intermediate, or dissociate to the products IO + NO_2. In the case of reaction 4, the excited adduct ($HOIO_2$*) can either dissociate back to OIO + OH or be stabilized to $HOIO_2$. For both reactions, the adduct energy was divided into a contiguous set of grains (width 30 cm^{-1}), each containing a bundle of rovibrational states. Each grain was then assigned a set of microcanonical rate coefficients for dissociation, which were determined using ILT to link them directly to $k_{\rm rec,\infty}$, the high-pressure limiting recombination coefficient.[28] ILT is particularly useful here because $k_{\rm rec,\infty}$ can be estimated using

TABLE 2: Geometries of the Stationary Points on the OIO + NO Potential Surface, Expressed in *Z* Matrix Notation

molecule	atom	no.[a]	N1	N2	N3	bond length[b]	angle[c]	dihedral angle[d]
OIONO	I	1						
	O	2	1			1.83		
	O	3	1	2		2.01	105.5	
	N	4	3	1	2	1.51	111.9	85.7
	O	5	4	3	1	1.15	109.4	−177.4
TS1	I	1						
	O	2	1			1.83		
	O	3	1	2		2.04	107.6	
	N	4	3	1	2	1.51	116.7	0.0
	O	5	4	3	1	1.15	108.7	180.0
TS2	I	1						
	O	2	1			1.92		
	O	3	1	2		1.93	63.1	
	N	4	2	1	3	3.11	54.1	163.5
	O	5	4	1	2	1.14	123.9	24.1
$IONO_2$	N	1						
	O	2	1			1.20		
	O	3	1	2		1.20	131.3	
	O	4	1	3	2	1.45	110.5	180.0
	I	5	4	1	2	2.03	117.3	0.0

[a] Atom number, see Figure 6. [b] Between atom and N1, in angstroms. [c] Between atom, N1 and N2. [d] Between atom, N1, N2, and N3.

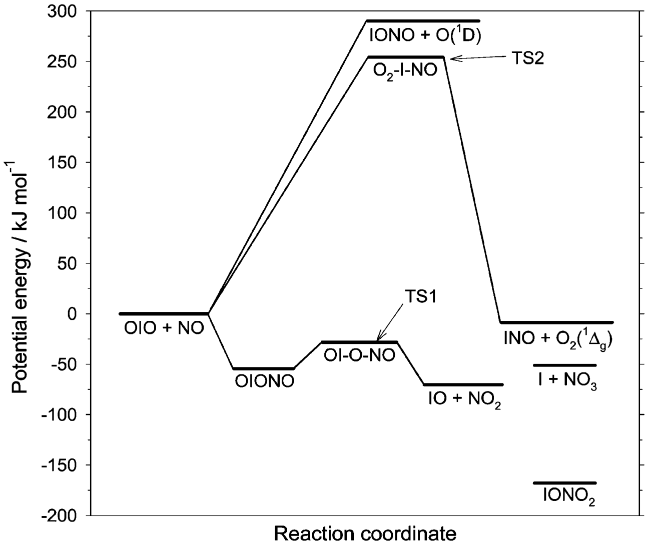

Figure 5. Potential-energy surface for the OIO + NO reaction. The geometries of the stationary points are illustrated in Figure 4.

long-range capture theory, assuming there are no energy barriers for these radical−radical reactions. For reaction 3, this is dominated by the dipole of OIO (3.89 D at the B3LYP/6-311+g(2d,p) level of theory) inducing a dipole in NO (polarizability = 1.7 × 10^{-24} cm^3).[29] The dipole−induced dipole capture rate[30] is then $k_{rec,\infty} = 2.7 \times 10^{-10} \exp(-46/T)$ cm^3 molecule^{-1} s^{-1}. For reaction 4, the dominant long-range force is between the dipole of OIO and that of OH (1.77 D[29]). This results in $k_{rec,\infty} = 5.5 \times 10^{-10} \exp(46/T)$ cm^3 molecule^{-1} s^{-1}, calculated using a recent implementation of long-range variational transition state theory.[31]

The density of states of the adduct was calculated using a combination of the Beyer−Swinehart algorithm for the vibrational modes (without making a correction for anharmonicity) and a classical densities of states treatment for the rotational modes.[32] The ME describes the evolution with time of the adduct grain populations. The probability of collisional transfer between grains was estimated using the exponential down model,[32] where the average energy for downward transitions, $\langle \Delta E \rangle_{down}$, was set to a typical value for N_2 at 300 K of 250 cm^{-1}.[32] The collision frequency between the adduct and N_2 was calculated using an intermolecular potential described by the parameters $\sigma = 3.5$ Å and $\epsilon/k = 350$ K. To use the ME to simulate irreversible stabilization of the adduct, an absorbing boundary was set 50 kJ mol^{-1} below the energy of the reactants, so that collisional energization from the boundary to the threshold was highly improbable. The absorbing boundary is used to limit the size of the matrixes involved in the RRKM calculation; for both reactions, it was verified that the resulting rate coefficients were essentially independent of the depth of the boundary when this was raised by 20 kJ mol^{-1}.

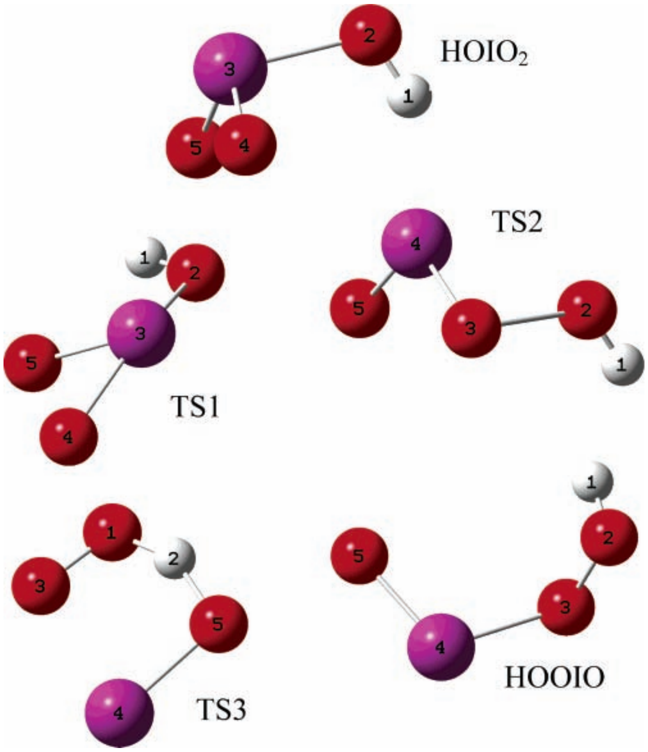

Figure 6. Geometries of stationary points on the OIO + OH potential-energy surface. The geometries are listed in *Z* matrix format in Table 4, and their relative energies are illustrated in Figure 7.

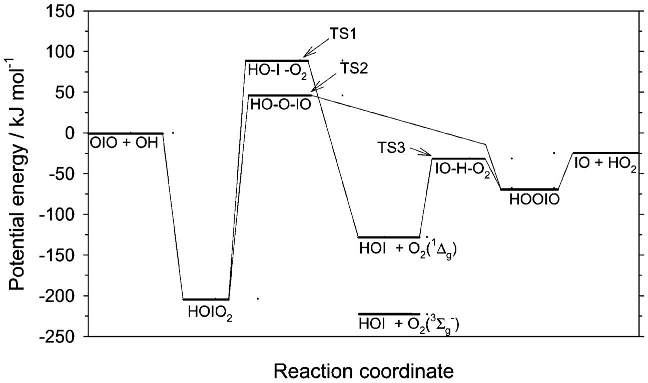

Figure 7. Potential-energy surface for the OIO + OH reaction. The geometries of the stationary points are illustrated in Figure 6.

Discussion

Reaction of OIO with NO. The OIO + NO potential-energy surface is illustrated in Figure 5. It should be noted that theoretical calculations on some sections of this surface have been published recently,[33,34] with which the present study is in good agreement. The most exothermic potential product is

TABLE 3: Calculated Vibrational Frequencies, Rotational Constants, and Energies of the Stationary Points and Asymptotes on the OIO + NO Singlet Potential-Energy Surface

species	vibrational frequencies[a]	rotational constants[b]	potential energy[c]
OIO + NO	273, 809, 831 and 1955	18.31, 7.05, 5.09 and 51.41	0
OIONO	73, 152, 188, 235, 388, 477, 800, 848, 1811	9.36, 1.42, 1.29	−55
OI-O-NO TS1	−126, 117, 147, 226, 347, 457, 787, 823, 1787	8.72, 1.45, 1.24	−28
IO + NO_2	648 and 762, 1382, 1672	9.84 and 241.3, 13.05, 12.38	−70
$IONO_2$	114, 177, 366, 588, 728, 753, 826, 1311, 1703	12.36, 1.305, 1.180	−166
I + NO_3	254, 267, 805, 1103, 1112, 1126	13.85, 13.82, 6.918	−50
IONO + O	170, 385, 407, 784, 853, 1649	16.89, 2.20, 1.94	101
ON-I-O2 TS2	570*i*, 54, 101, 150, 181,411,579, 716, 1870	7.14, 1.84, 1.45	254
INO + $O_2(^1\Delta_g)$	240, 517, 1857 and 1629	86.77, 2.80, 2.71 and 43.28	−10

[a] In cm^{-1}. [b] In GHz. [c] In kJ mol^{-1}, including zero-point energy and spin−orbit coupling of I and IO (see text).

TABLE 4: Geometries of the Stationary Points on the OIO + OH Potential Surface, Expressed in *Z* Matrix Notation

molecule	atom	no.[a]	N1	N2	N3	bond length[b]	angle[c]	dihedral angle[d]
$HOIO_2$	H	1						
	O	2	1			0.97		
	I	3	2	1		1.96	109.3	
	O	4	3	2	1	1.79	101.9	55.8
	O	5	3	2	1	1.79	101.9	−55.8
TS1	H	1						
	O	2	1			0.97		
	I	3	2	1		2.03	110.2	
	O	4	3	2	1	1.93	145.4	59.4
	O	5	4	2	1	2.05	56.5	−43.8
TS2	H	1						
	O	2	1			0.97		
	O	3	2	1		2.03	121.5	
	I	4	3	2	1	1.83	82.3	−130.6
	O	5	4	2	1	1.81	109.6	90.4
TS3	O	1						
	H	2	1			1.16		
	O	3	1	2		1.34	102.1	
	I	4	3	1	2	2.29	101.9	−23.9
	O	5	3	1	2	2.70	60.3	−9.7
HOOIO	H	1						
	O	2	1			0.97		
	O	3	2	1		1.44	101.3	
	I	4	3	2	1	2.03	111.8	−98.1
	O	5	3	2	1	3.08	101.4	−63.1

[a] Atom number, see Figure 6. [b] Between atom and N1, in angstroms. [c] Between atom, N1 and N2. [d] Between atom, N1, N2 and N3.

$IONO_2$. However, this cannot form from the addition of OIO to NO, because a cyclic transition state of very high energy would be required. The formation of I + NO_3 is prevented for the same reason. The abstraction by NO of the iodine atom from OIO is exothermic, even if spin is conserved and INO + $O_2(^1\Delta_g)$ is formed. However, this channel also has a substantial energy barrier. The only reaction pathway at the temperature range of the present study is therefore association of OIO and NO to form a weakly bound OIONO adduct, which then dissociates over a barrier to IO + NO_2 (reaction 3a). This picture is consistent with the observed kinetics: k_3 is independent of pressure over more than a 3-fold change in pressure, indicating that recombination to OIONO or $IONO_2$ is not important. The small negative temperature dependence of k_3 (eq II) is also characteristic of a reaction that proceeds via a shallow complex.

When the RRKM theory described above was applied to reaction 3, the single adjustable parameter was the height of the barrier between the OIONO adduct and the products IO + NO_2 (Figure 4). The quantum calculations predict this to be 28 kJ mol^{-1} below the energy of the reactants OIO + NO, with an uncertainty of ±16 kJ mol^{-1} at the level of theory employed.[35] A satisfactory fit to the experimental data, as shown in Figure 3, is obtained when the barrier height is raised by 10.5 kJ mol^{-1} to be 17.5 kJ mol^{-1} below the reactant energy. The RRKM calculation now reproduces both the absolute magnitude of k_3 and the small negative temperature dependence. If the barrier height is not raised, then the only way to match k_3 is to reduce $k_{rec,\infty}$. For instance, the experimental k_3(240 K) can be calculated by reducing $k_{rec,\infty}$ by a factor of ∼20 from the dipole−induced dipole capture frequency. However, there are no obvious reasons for doing this; furthermore, the RRKM calculation then predicts that k_3 has almost no temperature dependence, so that the rate constant is 70% higher than the experimental value at 320 K. With the higher barrier, the OIONO* energized adduct most likely dissociates back to OIO and NO at these pressures, rather than being quenched to OIONO or dissociating over the barrier to IO + NO_2.

Figure 8 illustrates the calculated rate coefficients for the OIONO association and IO + NO_2 atom abstraction channels, as a function of pressure at 300 K. This shows that even at atmospheric pressure (760 Torr), OIONO formation is almost 2 orders of magnitude slower. In any case, the barrier to IO + NO_2 is only 40.5 kJ mol^{-1} above the OIONO minimum, so that even if the adduct forms it will dissociate to IO + NO_2 very rapidly. Figure 8 also shows that the direct atom abstraction channel has a very small pressure dependence, in accord with the experimental measurements. For the purpose of atmospheric modeling, the recommended rate coefficient at 1 atm is

$$k_3(240 - 320\ \mathrm{K}) = (1.1 \pm 0.4) \times 10^{-12} \exp((542 \pm 130)/T)\ \mathrm{cm^3\ molecule^{-1}\ s^{-1}} \quad \text{(III)}$$

where the uncertainties are consistent with the experimental uncertainty (eq II).

Finally, it is interesting to compare the rate coefficient of (6.0 ± 1.1) × 10^{-12} cm^3 $molecule^{-1}$ s^{-1} measured here for OIO + NO at 300 K, with rate coefficients of 3.4 × 10^{-13} and 1.8 × 10^{-12} cm^3 $molecule^{-1}$ s^{-1} at 300 K for the analogous reactions for OClO[19] and OBrO,[18] respectively. Thus, the halogen dioxide + NO reactions become significantly faster down Group VII, in contrast to the reactions of the halogen monoxides with NO, which all have rate coefficients of about 2 × 10^{-11} cm^3 $molecule^{-1}$ s^{-1} at 300 K.[36]

Reaction of OIO with OH. The potential-energy surface for this reaction (Figure 7) shows that the formation of $HOIO_2$ can occur by the simple addition of OH to OIO (reaction 4a), promoted by the substantial long-range attraction between the large dipole moments of OH and OIO (see above). The predicted geometry of $HOIO_2$, and its stability with respect to these products, are in good accord with another recent theoretical study which focused on the reaction pathways of the HO_2 + IO reaction.[20] Experiments[37,38] have shown that the rate coefficient for this reaction has a negative activation energy similar

TABLE 5: Calculated Vibrational Frequencies, Rotational Constants, and Energies of the Stationary Points and Asymptotes on the OIO + OH Singlet Potential-Energy Surface

species	vibrational frequencies[a]	rotational constants[b]	potential energy[c]
OIO + OH	273, 809, 831 and 3707	18.31, 7.05, 5.09 and 558.7	0
$HOIO_2$	74, 258, 274, 303, 589, 875, 905, 977, 3734	5.69, 5.36, 3.63	−204
HOOIO	77, 212, 264, 378, 519, 796, 866, 1387, 3736	9.14, 2.77, 2.23	−68
HO−O−IO transition state	436*i*,113, 264, 280, 327, 762, 798, 856, 3720	7.59, 3.32, 2.90	46
IO + HO_2	648 and 1167, 1436, 3604	9.84 and 619.1, 33.68, 31.94	−25
HO−I−O_2 transition state	675*i*, 142, 231, 282, 522, 611, 737, 935, 3800	9.30, 4.02, 2.92	89
HOI + $O_2(^1\Delta_g)$	603, 1084, 3803 and 1629	623.9, 8.18, 8.08 and 43.28	−129

[a] In cm^{-1}. [b] In GHz. [c] In kJ mol^{-1}, including zero-point energy and spin−orbit coupling of I and IO (see text).

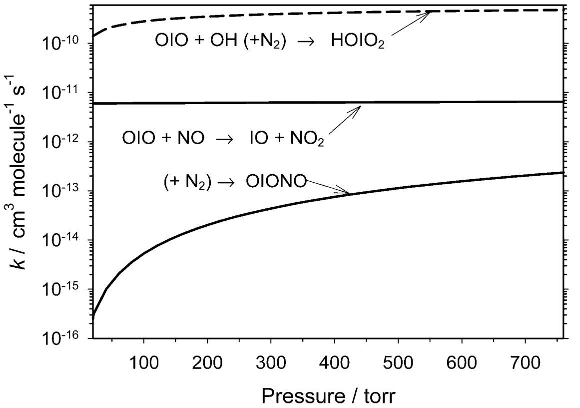

Figure 8. RRKM calculations at 300 K of the pressure dependences of the atom abstraction and recombination channels of reaction 3 and the recombination channel of reaction 4.

to the present result for reaction 3 (eq II). The kinetic behavior of the HO_2 + IO reaction is interpreted as proceeding through the HOOIO (and possibly HOOOI) intermediate and then forming $HOIO_2$ or dissociating to HOI + O_2.[20]

In the case of reaction 4, however, there are significant barriers to forming the possible exothermic products, HOI + $O_2(^1\Delta_g)$ and HO_2 + IO (Figure 7). Thus, recombination to form $HOIO_2$ is likely to be the only major channel at atmospheric temperatures. The RRKM model described above was then used to calculate k_4, the recombination rate coefficient, over a range of temperature (200−400 K) and pressure (0−1000 Torr). The results were fitted to the Lindemann expression modified by a broadening factor F_c

$$k_4 = \frac{k_{rec,0}[M]}{1 + \dfrac{k_{rec,0}[M]}{k_{rec,\infty}}} F_c^{\,K}$$

where

$$K = \frac{1}{\left\{1 + \left(\log_{10}\left(\dfrac{k_{rec,0}[M]}{k_{rec,\infty}}\right)\right)^2\right\}} \qquad \text{(IV)}$$

where the low-pressure limiting rate coefficient, $k_{rec,0} = 1.5 \times 10^{-27}\ (T/300\ K)^{-3.93}$ cm^6 $molecule^{-2}$ s^{-1}, and the high-pressure limiting rate coefficient, $k_{rec,\infty} = 5.5 \times 10^{-10} \exp(46/T)$ cm^3 $molecule^{-1}$ s^{-1}, are obtained from the RRKM calculation. The best fit yields $F_c = 0.30$, which is somewhat smaller than the value of 0.6 often assumed.[36]

The falloff curve for reaction 4a at 300 K is shown in Figure 8; the reaction is predicted to be close to the high-pressure limit at pressures above 20 Torr. For the purpose of atmospheric modeling, the predicted rate coefficient at 1 atm pressure is

$$k_4(240 - 320\ K) = 2.2 \times 10^{-10} \exp(243/T)\ cm^3\ molecule^{-1}\ s^{-1} \qquad \text{(V)}$$

We have considered three sources of uncertainty in this RRKM prediction: an uncertainty of ±16 kJ mol^{-1} [35] in the calculated binding energy of OIO and OH, a ±20% uncertainty in the lowest vibrational frequency of $HOIO_2$ (Table 4), and an uncertainty of ±100 cm^{-1} in $\langle \Delta E \rangle_{down}$. By combination in quadrature the effects of these uncertainties on the RRKM calculation, the estimated uncertainty of k_4 in eq V varies from ±11% at 240 K to ±22% at 320 K.

The analogous reaction OH + OClO has been studied in a fast-flow tube.[39] A rate coefficient of $4.5 \times 10^{-13} \exp(804/T)$ cm^3 $molecule^{-1}$ s^{-1} was measured, and it was shown that the major product channel (at about 1 Torr pressure) was HOCl + O_2. A theoretical study[40] of the potential-energy surface of this reaction shows that the relevant barrier (analogous to TS1 in Figure 7) is below the energy of the reactants, allowing the bimolecular reaction to proceed. This is an interesting contrast with reaction 4.

Atmospheric Implications. In the Introduction, we demonstrated that field observations of IO and OIO indicate that the OIO lifetime during the day in the clean coastal marine boundary layer is less than 140 s. To gauge an upper limit to the importance of reactions 3 and 4, first ignore photolysis of OIO and recombination with IO to form I_2O_3. Taking our measured value for k_3 at 290 K, then the absence of detectable levels of OIO (<3 ppt) could be due to the presence of more than just 50 ppt of NO. Although there is not sufficient OH in the marine boundary layer to control the OIO concentration through reaction 4, a typical summertime average OH concentration during the day of 1×10^6 cm^{-3} would cause ~5% of OIO to form $HOIO_2$. If $HOIO_2$ was then removed only by uptake on aerosol, this would provide an important route to aerosol iodate.

Conclusions

In this paper, we have explored the reactions of OIO with NO and OH. The rate coefficient for OIO + NO was determined experimentally and that for OIO + OH by RRKM theory using quantum calculations of the relevant points on the potential-energy surface. The rate coefficients of both reactions are fast enough around 290 K and 1 atm pressure for these reactions to play a potentially important role in the gas phase and aerosol chemistry in the marine boundary layer of the atmosphere.

In addition, these radical−radical reactions make an interesting contrast. OIO + NO can form a weakly bound OIONO intermediate, which then dissociates to the products IO + NO_2. However, the most stable potential product, $IONO_2$, cannot form because of the significant rearrangement of OIONO that would be required. In contrast, OIO + OH can form directly the very stable $HOIO_2$ molecule, but the bimolecular reaction channels to $HO_2 + IO$ and $HOI + O_2$ are closed because of significant energy barriers.

Acknowledgment. This work was supported by the UK Natural Environment Research Council under the COSMAS initiative and by the THALOZ project funded by the European Commission.

References and Notes

(1) Alicke, B.; Hebestreit, K.; Stutz, J.; Platt, U. *Nature* **1999**, *397*, 572.

(2) Allan, B. J.; McFiggans, G.; Plane, J. M. C.; Coe, H. *J. Geophys. Res.-Atmos.* **2000**, *105*, 14363.

(3) Saiz-Lopez, A.; Plane, J. M. C. *Geophys. Res. Lett.* **2004**, *31*, art. no.

(4) Allan, B. J.; Plane, J. M. C.; McFiggans, G. *Geophys. Res. Lett.* **2001**, *28*, 1945.

(5) Davis, D. J.; Crawford, J.; Liu, S.; McKeen, S.; Bandy, A.; Thornton, D.; Rowland, F.; Blake, D. *J. Geophys Res.* **1996**, *101*, 2135.

(6) McFiggans, G.; Plane, J. M. C.; Allan, B. J.; Carpenter, L. J.; Coe, H.; O'Dowd, C. *J. Geophys. Res.-Atmos.* **2000**, *105*, 14371.

(7) Vogt, R.; Sander, R.; Von Glasow, R.; Crutzen, P. J. *J. Atmos. Chem.* **1999**, *32*, 375.

(8) McFiggans, G.; Cox, R. A.; Mossinger, J. C.; Allan, B. J.; Plane, J. M. C. *J. Geophys. Res.-Atmos.* **2002**, *107*, art. no. 4271.

(9) Jimenez, J. L.; Bahreini, R.; Cocker, D. R.; Zhuang, H.; Varutbangkul, V.; Flagan, R. C.; Seinfeld, J. H.; O'Dowd, C. D.; Hoffmann, T. *J. Geophys. Res.-Atmos.* **2003**, *108*, art. no. 4318.

(10) O'Dowd, C. D.; Jimenez, J. L.; Bahreini, R.; Flagan, R. C.; Seinfeld, J. H.; Hameri, K.; Pirjola, L.; Kulmala, M.; Jennings, S. G.; Hoffmann, T. *Nature* **2002**, 632.

(11) McFiggans, G.; Coe, H.; Burgess, R.; Allan, J.; Cubison, M.; Alfarra, M. R.; Saunders: R.; Saiz-Lopez, A.; Plane, J. M. C.; Wevill, D. J.; Carpenter, L. J.; Rickard, A. R.; Monks, P. S. *Atmos. Chem. Phys.* **2004**, *4*, 701.

(12) Carpenter, L. J.; Malin, G.; Liss, P. S.; Kupper, F. C. *Glob. Biogeochem. Cycle* **2000**, *14*, 1191.

(13) Cox, R. A.; Bloss, W. J.; Jones, R. L.; Rowley, D. M. *Geophys. Res. Lett.* **1999**, *26*, 1857.

(14) Joseph, D. M.; Ashworth, S. H.; Plane, J. M. C. *J. Photochem. Photobiol., A* **2005**, *176*, 68.

(15) Rowley, D. M.; Bloss, W. J.; Cox, R. A.; Jones, R. L. *J. Phys. Chem. A* **2001**, *105*, 7855.

(16) Ashworth, S. H.; Allan, B. J.; Plane, J. M. C. *Geophys. Res. Lett.* **2002**, *29*.

(17) Saiz-Lopez, A.; Plane, J. M. C.; McFiggans, G.; Ball, S. M.; Bitter, M.; Jones, R. L. *Atmos. Chem. Phys. Discuss.* **2005**, *5*, 5405.

(18) Li, Z. J.; Tao, Z. N. *Chem. Phys. Lett.* **1999**, *306*, 117.

(19) Li, Z. J.; Wuebbles, R. D.; Pylawka, N. J. *Chem. Phys. Lett.* **2002**, *354*, 491.

(20) Drougas, E.; Kosmas, A. M. *J. Phys. Chem. A* **2005**, *109*, 3887.

(21) Baker, A. R.; Tunnicliffe, C.; Jickells, T. D. *J. Geophys. Res.-Atmos.* **2001**, *106*, 28743.

(22) Ley, L.; Masanet, J.; Caralp, F.; Lesclaux, R. *J. Phys. Chem.* **1995**, *99*, 1953.

(23) Gilles, M. K.; Burkholder, J. B.; Ravishankara, A. R. *Int. J. Chem. Kinet.* **1999**, *31*, 417.

(24) Frisch, M. J.; Trucks, G. W.; Schlegel, H. B.; Scuseria, G. E.; Robb, M. A.; Cheeseman, J. R.; J. A. Montgomery, J.; Vreven, T.; Kudin, K. N.; Burant, J. C.; Millam, J. M.; Iyengar, S. S.; Tomasi, J.; Barone, V.; Mennucci, B.; Cossi, M.; Scalmani, G.; Rega, N.; Petersson, G. A.; Nakatsuji, H.; Hada, M.; Ehara, M.; Toyota, K.; Fukuda, R.; Hasegawa, J.; Ishida, M.; Nakajima, T.; Honda, Y.; Kitao, O.; Nakai, H.; Klene, M.; Li, X.; Knox, J. E.; Hratchian, H. P.; Cross, J. B.; Adamo, C.; Jaramillo, J.; Gomperts, R.; Stratmann, R. E.; Yazyev, O.; Austin, A. J.; Cammi, R.; Pomelli, C.; Ochterski, J. W.; Ayala, P. Y.; Morokuma, K.; Voth, G. A.; Salvador, P.; Dannenberg, J. J.; Zakrzewski, V. G.; Dapprich, S.; Daniels, A. D.; Strain, M. C.; Farkas, O.; Malick, D. K.; Rabuck, A. D.; Raghavachari, K.; Foresman, J. B.; Ortiz, J. V.; Cui, Q.; Baboul, A. G.; Clifford, S.; Cioslowski, J.; Stefanov, B. B.; Liu, G.; Liashenko, A.; Piskorz, P.; Komaromi, I.; Martin, R. L.; Fox, D. J.; Keith, T.; Al-Laham, M. A.; Peng, C. Y.; Nanayakkara, A.; Challacombe, M.; Gill, P. M. W.; Johnson, B.; Chen, W.; Wong, M. W.; Gonzalez, C.; Pople, J. A. *Gaussian 03*, Revision B.03; Gaussian Inc.: Pittsburgh, PA, 2003.

(25) Glukhovtsev, M. N.; Pross, A.; McGrath, M. P.; Radom, L. *J. Chem. Phys.* **1995**, *103*, 1878.

(26) Chase, M. W.; Davies, C. A.; Downey, J. R.; Frurip, D. J.; A., M. R.; Syverud, A. N. *J. Phys. Chem. Ref. Data* **1985**, *14*.

(27) Bedjanian, Y.; Le Bras, G.; Poulet, G. *J. Phys. Chem. A* **1997**, *101*, 4088.

(28) De Avillez Pereira, R.; Baulch, D. L.; Pilling, M. J.; Robertson, S. H.; Zeng, G. *J. Phys. Chem.* **1997**, *101*, 9681.

(29) Lide, D. R. *Handbook of Physics and Chemistry*, 72rd ed.; CRC Press: Boca Raton, FL, 1992.

(30) Maitland, G. C.; Rigby, M.; Smith, E. B.; Wakeham, W. A. *Intermolecular Forces Their Origin and Determination*; Oxford University Press: Oxford, 1981.

(31) Georgievskii, Y.; Klippenstein, S. J. *J. Chem. Phys.* **2005**, *122*, art. no. 194103.

(32) Gilbert, R. G.; Smith, S. C. *Theory of Unimolecular and Recombination Reactions*; Blackwell: Oxford, 1990.

(33) Papayannis, D. K.; Kosmas, A. M. *Chem. Phys. Lett.* **2004**, *398*, 75.

(34) Papayannis, D. K.; Kosmas, A. M. *Chem. Phys.* **2005**, *315*, 251.

(35) Foresman, J. B.; Frisch, A. *Exploring chemistry with electronic structure methods*; Gaussian, Inc.: Pittsburgh, PA, 1996.

(36) Sander, S. P.; Friedl, R. R.; Golden, D. M.; Kurylo, M. J.; Huie, R. E.; Orkin, V. L.; Moortgat, G. K.; Ravishankara, A. R.; Kolb, C. E.; Molina, M. J.; Finlayson-Pitts, B. J. *Chemical Kinetics and Photochemical Data for Use in Stratospheric Modelling: Evaluation 14*; JPL Publication 02-25: Pasadena, 2002.

(37) Cronkhite, J. M.; Stickel, R. E.; Nicovich, J. M.; Wine, P. H. *J. Phys. Chem. A* **1999**, *103*, 3228.

(38) Knight, G. P.; Crowley, J. N. *Phys. Chem. Chem. Phys.* **2001**, *3*, 393.

(39) Poulet, G.; Zagogianni, H.; Lebras, G. *Int. J. Chem. Kinet.* **1986**, *18*, 847.

(40) Xu, Z.-F.; Zhu, R.; Lin, M. C. *J. Phys. Chem. A* **2003**, *107*, 1040.